

Few distinguishable particles with an impurity in a one-dimensional harmonic trap

A. Rojo-Francàs^{1,2}, F. Isaule³, and B. Juliá-Díaz^{1,2}

¹ Departament de Física Quàntica i Astrofísica, Facultat de Física, Universitat de Barcelona, Martí i Franquès 1, E-08028 Barcelona, Spain

² Institut de Ciències del Cosmos (ICCUB), Universitat de Barcelona, Martí i Franquès 1, E-08028 Barcelona, Spain

³ School of Physics and Astronomy, University of Glasgow, Glasgow G12 8QQ, United Kingdom

E-mail: bruno@fqa.ub.edu

December 2022

Abstract. We study the static properties of a mobile impurity interacting with a bath with a few distinguishable particles trapped in a one-dimensional harmonic trap. We focus on the limiting case where the bath is non-interacting. We provide numerical results for the energy spectra and density profiles by means of the exact diagonalization of the Hamiltonian, and find that these systems show non-trivial solutions, even in the limit of infinite repulsion. A detailed physical interpretation is provided for the lowest energy states. In particular, we find a seemingly universal transition from the impurity being localized in the center of the trap to being expelled outside the majority cloud. A mean-field approach is developed which captures the transition.

Submitted to: *New J. Phys.*

1. Introduction

The study of impurities interacting with a quantum bath is of relevance in many branches of physics. Examples range from the famous problems of electrons coupled to ionic crystals [1] and ³He impurities in liquid Helium [2, 3] to nucleon impurities in neutron matter [4]. More recently, ultracold atom experiments [5, 6] have opened a new avenue for probing impurities in quantum baths, offering a unique setting to control impurity-bath systems. In particular, both Fermi [7, 8] and Bose [9, 10] polarons have already been observed experimentally, and the realization of more sophisticated impurity systems is expected in the near future.

The mentioned developments have motivated extensive theoretical studies of impurities in a variety of configurations, including different statistics [11, 12] and dimensions [13–16]. These studies can further test the validity of our theoretical

approaches and bridge the gap between few- and many-body physics. Indeed, the important impact of impurity-bath correlations means that perturbative approaches are often not reliable, especially in strongly-interacting regimes, requiring us to rely on more sophisticated theoretical techniques.

In this direction, one-dimensional gases [17, 18] offer a unique platform to study impurities [19–27]. Fluctuations are enhanced in one-dimension, increasing the importance of impurity-bath correlations. Furthermore, one-dimensional systems often offer us reliable solutions, such as from the Bethe ansatz [28] or from numerical diagonalization of few-particles systems [29, 30]. Experimentally, ultracold atoms have provided realizations of one-dimensional gases for two decades [31, 32], including the observation of impurity dynamics [33].

Significant theoretical efforts have been put to understand the behavior of impurities in one-dimensional harmonic traps [34–42], as they better simulate experimental conditions. In particular, in this work, we are concerned with the study of impurities in a bath with a few particles, which can be studied with exact diagonalization (ED) techniques [43]. Even though ED calculations are restricted to a small number of particles, they provide us with highly accurate results for many properties, including the low-energy spectrum and density profiles. These studies can then provide helpful insight into systems with more particles.

In this work, we study a one-dimensional harmonic trap loaded with one mobile impurity interacting repulsively with a bath of a few (two to seven) distinguishable and non-interacting particles. This configuration contrasts with related studies with baths of single-component bosons [34]. We note that a similar configuration as the one we consider has been studied in [35], where one particle interacts with a small bath of non-interacting identical bosons. In particular, Ref. [35] provides an analytical result for three particles in the limit of infinite repulsion. We employ this analytical solution to benchmark our calculations.

We report an exhaustive examination of the low-energy spectrum and density profiles of the branch of repulsive interactions by performing ED calculations for harmonic traps [44–46]. Even though, and despite the name, the results are not exact, we improve the quality of our results by renormalizing the interactions with the known two-body solution, as explained in detail in Ref. [47]. We compare our numerical calculations with mean-field (MF) solutions in the regime of weak repulsion, while we also propose an ansatz for the ground state in the limit of infinite repulsion. We find that the properties of the system saturate to non-trivial solutions for strong interactions, which are correctly captured by our analytical ansatz. We also examine the dependence of the energy and density profiles on the number of particles to provide insight into many-body scenarios.

As shown by similar works [34], while for weak repulsion the bath and impurity are localized at the center of the trap, for strong repulsion above a critical interaction strength the bath expels the impurity to the borders of the trap. This impurity-bath separation can be qualitatively understood as if the impurity was trapped in a double well, i.e. the bath particles localized in the center of the trap play the role of the

central barrier. We characterize the transition between the two regimes by studying the position of the maximum of impurity density, which goes from zero to a finite value. In addition, we find that the critical interaction strength for this separation shows a universal behavior in baths with a different number of particles.

This work is organized as follows. In section 2 we present our model and numerical considerations. We also present the complementary MF approach and the ansatz for infinite repulsion. In section 3 we examine the energies of the system for a wide range of interaction strengths, with a detailed analysis of both the ground state and the low-energy spectrum. Afterward, in section 4 we examine the ground-state density profiles for a representative set of the number of particles and interaction strengths. Finally, in section 5 we present the main conclusions of our work and an outline for future directions.

2. Model

We consider a one-dimensional system with N distinguishable particles of equal mass m trapped in a harmonic potential and that interact through short-range potentials. We assume that one particle, the impurity, interacts with equal inter-atomic potentials with the other $N_b = N - 1$ particles, while the N_b particles in the *bath* do not interact among themselves. By approximating the impurity-bath interaction by an effective contact potential of strength g , the Hamiltonian takes the form

$$\hat{H} = \sum_{i=1}^N \left[-\frac{\hbar^2}{2m} \frac{\partial^2}{\partial x_i^2} + \frac{m\omega^2}{2} x_i^2 \right] + g \sum_{i \neq I}^{N_b} \delta(x_I - x_i), \quad (1)$$

where ω is the harmonic oscillator (HO) trapping frequency and the interaction strength is related to the one-dimensional s -wave scattering length a via $g = -2\hbar^2/a$. In the rest of this text, we employ lowercase letters to denote arbitrary particles, whereas we employ capital letters to denote a specific particle. From now on, we consider repulsive interactions $g > 0$, leaving the study of the attractive branch for future work.

We first stress that the solution in the non-interacting limit $g = 0$ is simply given by the textbook solution of the harmonic oscillator. In contrast, interacting systems $g \neq 0$ require more careful treatment, such as from a perturbative calculation or a numerical diagonalization. In this work, in a first instance, we perform exact diagonalizations (ED) of the Hamiltonian (1), where we employ many-body basis in the space of single-particle HO modes, which we truncate up to a chosen HO-mode cutoff. Within this truncated subspace, we diagonalize the Hamiltonian using standard numerical routines. We refer to Refs. [46, 48] for detailed reviews on the ED method for harmonic traps.

We stress that due to the use of a truncated basis, the results are not exact. Naturally, the quality of the results improves when we increase the number of HO modes. However, the number of possible basis states grows rapidly with the number of particles, restricting our calculations to a few particles. Nevertheless, to improve the quality of our results and to access systems with more particles, we renormalize the interaction

strengths, following the approach described in Ref. [47]. With this method, one corrects the value of the interaction strength used in the initial numerics to a more accurate physical one. This method is well tested in the symmetric cases of a few particles and, as we show later, it provides an excellent agreement with known analytical solutions for one impurity interacting with two bath particles.

2.1. Mean-field solution

To complement the ED calculations, we also study the weakly-interacting regime within a mean-field (MF) approximation. This enables us to gain further insight and examine systems with a large number of particles, which we cannot access with ED. We introduce the MF wavefunction

$$\Psi(x, x_1, \dots, x_N) = \phi(x) \prod_{i=1}^{N_b} \varphi^i(x_i), \quad (2)$$

where $\phi(x)$ is the impurity wavefunction and $\varphi^i(x_i)$ is the i -th bath particle wavefunction. By employing (2), we obtain the MF equations

$$\left(-\frac{\hbar^2}{2m} \frac{d^2}{dx^2} + \frac{m\omega^2}{2} x^2 + g \sum_i |\varphi^i(x)|^2 \right) \phi(x) = \epsilon_I \phi(x), \quad (3)$$

$$\left(-\frac{\hbar^2}{2m} \frac{d^2}{dx^2} + \frac{m\omega^2}{2} x^2 + g|\phi(x)|^2 \right) \varphi^i(x) = \epsilon_b \varphi^i(x) \quad i = 1, \dots, N_b, \quad (4)$$

where ϵ_I and ϵ_b are the eigenvalues of both equations and are used as the convergence parameter. We diagonalize Eqs. (3) and (4) self-consistently until they meet a convergence criteria for ϵ_I and ϵ_b . We can choose ground- or excited-state solutions depending on the chosen wavefunctions states during the self-consistent calculation. Naturally, in the ground state, all the wavefunctions of the bath are equal ($\varphi^i(x) = \varphi(x)$), and thus, the interaction term in (3) takes the form $gN_b|\varphi(x)|^2$. In contrast, one excited solution corresponds to having one bath's particle in its first excited state φ_1 , while the rest of the $N_b - 1$ particles in the bath are in their ground state φ_0 . In this case, the interaction term in (3) takes the form $g(N_b - 1)|\varphi_0(x)|^2 + g|\varphi_1(x)|^2$. Higher excited states behave analogously.

From the converged solutions for $\phi(x)$ and $\varphi^i(x_i)$, we extract the densities of each particle from $\rho_I(x) = |\phi(x)|^2$ and $\rho_i(x) = |\varphi^i(x)|^2$. In addition, we compute the energy from the functional

$$\begin{aligned} E_{\text{MF}} = & \int \phi^*(x) \left(-\frac{\hbar^2}{2m} \frac{d^2}{dx^2} + \frac{m\omega^2}{2} x^2 \right) \phi(x) dx \\ & + \sum_{i=1}^{N_b} \int \varphi^{i*}(x) \left(-\frac{\hbar^2}{2m} \frac{d^2}{dx^2} + \frac{m\omega^2}{2} x^2 \right) \varphi^i(x) dx \\ & + g \sum_{i=1}^{N_b} \int |\varphi^i(x)|^2 |\phi(x)|^2 dx. \end{aligned} \quad (5)$$

where we perform the derivatives and integrals numerically. We examine the energies in section 3 and the densities profiles in section 4.

2.2. Ansatz for infinite repulsion

Finally, we also complement the ED calculations for strong repulsion by proposing an ansatz for the wavefunction in the limit of infinite repulsion. By taking into account that in the limit $g \rightarrow \infty$ the impurity cannot be at the same position as any of the bath particles, we introduce an ansatz with Jastrow-like correlations [49]

$$\begin{aligned} \Psi_{N,\sigma}(x_I, x_i) = & \alpha_N e^{-x_I^2/2\sigma^2} \sum_{N_a=0}^{\lfloor N_b/2 \rfloor} \sum_P \prod_{i \neq j}^{2N_a} |x_I - x_i| |x_I - x_j| e^{-(x_i^2 + x_j^2)/2\sigma^2} \\ & \times \prod_{k \neq i,j}^{N_b - 2N_a} (x_I - x_k) e^{-x_k^2/2\sigma^2}, \end{aligned} \quad (6)$$

where x_I is the position of the impurity, x_b are the positions of the N_b bath particles, α_N is a normalization factor that depends on the number of particles N , and σ is a variational parameter that can be adjusted analytically. In the sums, N_a denotes the number of pairs of absolute values and P are the permutations of the index i, j with the index k .

We first note that (6) improves over a similarly inspired ansatz proposed in Ref. [43], which does not contain the terms with absolute values nor the σ parameter. The introduction of a linear combination of terms with $(x_I - x_i)(x_I - x_j)$ and $|x_I - x_i||x_I - x_j|$, as well as the introduction of the parameter σ , enable us to provide a more accurate variational solution. To understand this, we note that a simple ansatz without the linear combination results in the same energy as one with a different number of pairs of absolute values N_a . For example, both

$$\Psi(x_I, x_i) = \alpha(x_I - x_A)(x_I - x_B) e^{-(x_I^2 + x_A^2 + x_B^2)/2}, \quad (7)$$

and

$$\Psi(x_I, x_i) = \alpha |x_I - x_A| |x_I - x_B| e^{-(x_I^2 + x_A^2 + x_B^2)/2}, \quad (8)$$

result in the same energy. However, these wavefunctions are not orthogonal, and thus, a linear combination of them can give a better variational solution. We have found that the minimum energy is obtained when all the functions have the same weight.

As an example, the ansatz for three particles ($N_b = 2$) reads

$$\Psi_{3,\sigma}(x_I, x_A, x_B) = \alpha_3 ((x_I - x_A)(x_I - x_B) + |x_I - x_A||x_I - x_B|) e^{-(x_I^2 + x_A^2 + x_B^2)/2\sigma^2}, \quad (9)$$

where A and B denote the two particles in the bath. In this example, we have a first part with $N_a = 0$, i.e. without absolute values, and a second part with $N_a = 1$, i.e. with a pair of absolute values. For an increasing number of particles, the ansatz takes analogous, but more complicated forms. We provide examples for four and five particles in Appendix A.

The value of σ that minimizes the energy can be computed analytically as a function of the kinetic and potential energies for $\sigma = 1$. The total average energy of the state with the σ that minimizes it is

$$E(N) = 2\sqrt{E_{\text{kin.}}(\sigma = 1, N)E_{\text{pot.}}(\sigma = 1, N)}, \quad (10)$$

where $E_{\text{kin.}}(\sigma, N) = \langle \Psi_{N,\sigma} | \hat{H}_{\text{kin.}} | \Psi_{N,\sigma} \rangle$ and $E_{\text{pot.}}(\sigma, N) = \langle \Psi_{N,\sigma} | \hat{H}_{\text{pot.}} | \Psi_{N,\sigma} \rangle$, with $\hat{H}_{\text{kin.}}$ and $\hat{H}_{\text{pot.}}$ the kinetic and potential part of the Hamiltonian (1), respectively. We provide a more detailed derivation in Appendix A

3. Energy spectrum

We first examine the energies of the system for different interaction-strength regimes. In the following, we start by providing an exhaustive examination of the ground states, to then study the low-energy spectrum.

3.1. Ground-state energy for strong interactions

To analyze the ground-state energies, we study the energy increase of the system due to the impurity-bath interaction

$$E_{I_g}^N \equiv E(g, N) - E(g = 0, N), \quad (11)$$

where g simply indicates the interaction strength at which the energy is obtained and N is the number of particles employed. In related studies, $E_{I_g}^N$ is usually referred to as the polaron or binding energy of the impurity [9], which can be interpreted as the energy required to add the impurity to the system. We note that we examine the full energy in the next subsection.

We show values of $E_{I_g}^N$ obtained from ED calculations for up to $N = 8$ ($N_b = 7$) particles in figure 1. We plot the results as a function of the inverse of the interaction strength to focus on the strongly-interacting regime $g^{-1} \approx 0$. We also show exact results for $N = 3$ [35] (black circles), obtaining a perfect agreement. First, and as expected, we note that $E_{I_g}^N$ increases with increasing g , reaching non-trivial values for $g^{-1} \rightarrow 0$. Second, we find that $E_{I_g}^N$ also increases with N . We stress that by construction, $E_{I_0}^N = 0$ for all number of particles. Therefore, it requires more energy to add an impurity to a more populated and more repulsive bath.

We report the obtained values of $E_{I_g}^N$ at $g^{-1} \approx 0$ in table 3.1. We also report the corresponding energies obtained from the ansatz for infinite repulsion (6). We obtain a reasonable agreement between the values obtained from ED and the ansatz, especially for a small number of particles, showing that the proposed ansatz gives a good description of this configuration. However, the agreement decreases with an increase in the number of particles, reaching a difference of approximately 36% (14% for the total energy) for $N = 8$. We also stress that Ref. [35] found that the exact value for $N = 3$ corresponds to $E_{I_\infty}^3 = 3/2\hbar\omega$, in almost perfect agreement with our numerical calculations.

To further characterize the limit of infinite repulsion, we also report in table 3.1 the values obtained with ED for the derivative of $E_{I_g}^N$ at $g = 0$,

$$K = - \left[\frac{dE_I}{dg^{-1}} \right]_{g^{-1}=0}. \quad (12)$$

This magnitude is connected to Tan's contact [50] and can be used to compute the interaction energy as $E_{\text{int.}} = g^{-1}K$, as dictated by the Hellman-Feynman theorem. We

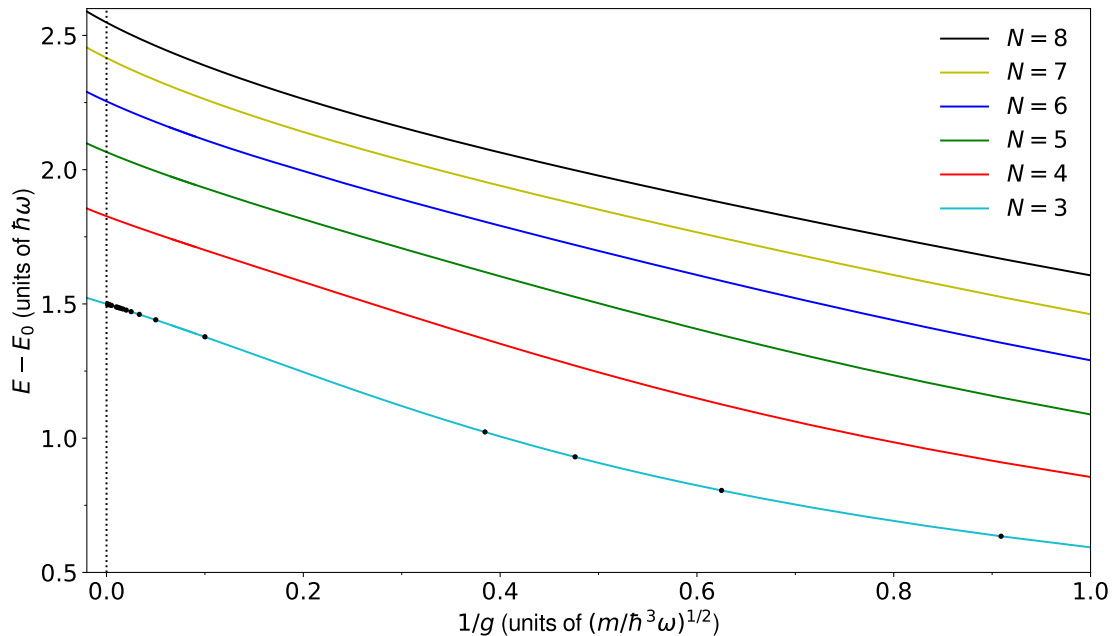


Figure 1. Ground-state energy $E_{I_g}^N$ as a function of the inverse of the interaction strength $1/g$. We show results for three to eight particles, as indicated in the labels. The solid lines correspond to results from ED, while the black circles correspond to the results reported in [35]. We have employed 90, 45, 30, 20, 15, and 15 HO modes for three, four, five, six, seven, and eight particles, respectively.

Table 1. Energies $E_{I_g}^N$ (in units of $\hbar\omega$) and derivatives K (in units of $(\hbar^5\omega^3/m)^{1/2}$) computed for $g^{-1} \approx 0$ for different number of particles N . The ED results (first and third lines) are obtained for $g = 1000(m/\hbar^3\omega)^{1/2}$. The second line shows the energies at $g^{-1} = 0$ obtained from ansatz (6).

N	3	4	5	6	7	8
$E_{I_\infty}^N$	1.499	1.826	2.064	2.253	2.415	2.549
$E_{I_{\text{ansatz}}}^N$	1.539	1.967	2.358	2.735	3.107	3.477
K	1.145	1.379	1.538	1.678	1.834	1.933

obtain that K increases with N , indicating that for large interactions (but not infinite) the interaction energy increases with the number of particles. We also note that Ref. [35] reported the exact value $K = \frac{9}{\sqrt{2\pi^3}} \approx 1.143$ for $N = 3$, also in almost perfect agreement with our numerical results.

Within the range of the number of particles examined, even though $E_{I_g}^N$ increases with N , we find that this increase becomes smaller with larger baths. Indeed, we find that

$$E_{I_\infty}^{N+1} - E_{I_\infty}^N > E_{I_\infty}^{N+2} - E_{I_\infty}^{N+1}. \quad (13)$$

which can be appreciated in both figure 1 and table 3.1. To provide energy estimates for systems with many particles, we fit the obtained numerical energies at $g^{-1} \approx 0$ to

the function

$$E_{I\infty}^N = \Delta E \left(1 - \frac{1}{N^b}\right), \quad (14)$$

where ΔE and b are parameters determine. The best fit for our numerical results gives $\Delta E = 6.7 \pm 0.2$ and $b = 0.228 \pm 0.009$, showing that our results are well adjusted by function (14).

The parameter ΔE gives an estimate for the value of E_I for an infinite number of particles at the infinite repulsion limit. Because ΔE is finite, we find that $E_{I\infty}$ saturates for large N . Naturally, the total ground-state energy of the system E diverges for infinite N . However, the energy required to add an impurity saturates. Nevertheless, this extrapolation should be taken with care and should be contrasted with a robust many-body calculation in the future.

3.2. Energy spectrum

Having examined the ground state, we now turn our attention to the full energy in the lower part of the spectrum. In figure 2 we show the low-energy spectrum as a function of g for three to six particles. We also show exact results for $N = 3$ from Ref. [35], in perfect agreement with our numerical results. We highlight the center-of-mass excitations with red lines which arise from the separability of the center-of-mass Hamiltonian [51]. These excitations have an energy gap of $n\hbar\omega$ ($n = 1, 2, \dots$) with respect to the ground state or intrinsic excitations.

Naturally, in the non-interacting limit $g = 0$, the energy spectrum is simply given by the HO solution $E_n(g = 0) = \hbar\omega \sum_a^N (n_a + 1/2)$. In contrast, for strong repulsion, the spectra saturate to non-trivial values which do not correspond to eigenvalues of the HO Hamiltonian.

In the non-interacting limit $g = 0$, the energies show the expected degeneracies for N distinguishable particles in a harmonic oscillator. Some of these degeneracies are lifted for $g \neq 0$, as seen in panels (a-d) of figure 2. However, in the limit $g \rightarrow +\infty$ new degeneracies are introduced.

Indeed, in the strongly interacting limit, $g \rightarrow +\infty$, the ground state becomes double degenerate in all cases, with one even and one odd parity states (see right part of panels (a-d) of figure 2). In this limit, the first excitation (lowest blue lines in all panels) is a center-of-mass excitation of the ground-state doublet and has an energy gap of $\hbar\omega$ for all values of g . Slightly above the lowest center-of-mass excitation (for $g \rightarrow \infty$), the spectrum shows an intrinsic excitation. For $N = 3$, this intrinsic excitation is created by a manifold of four states and reaches the Tonks-Girardeau energy for three particles, $E = 9/2\hbar\omega$. For $N > 3$, this intrinsic excitation is instead created by a doublet structure of opposite parity. Each line of the doublet is itself degenerate $D = N - 2$ times. It is worth mentioning that this first intrinsic excited doublet (see panels (b-d) of figure 2) is only present if the bath is made by distinguishable particles. A system with a bath of identical bosons shows the same ground state doublet (and some excitations) but not this intrinsic excitation.

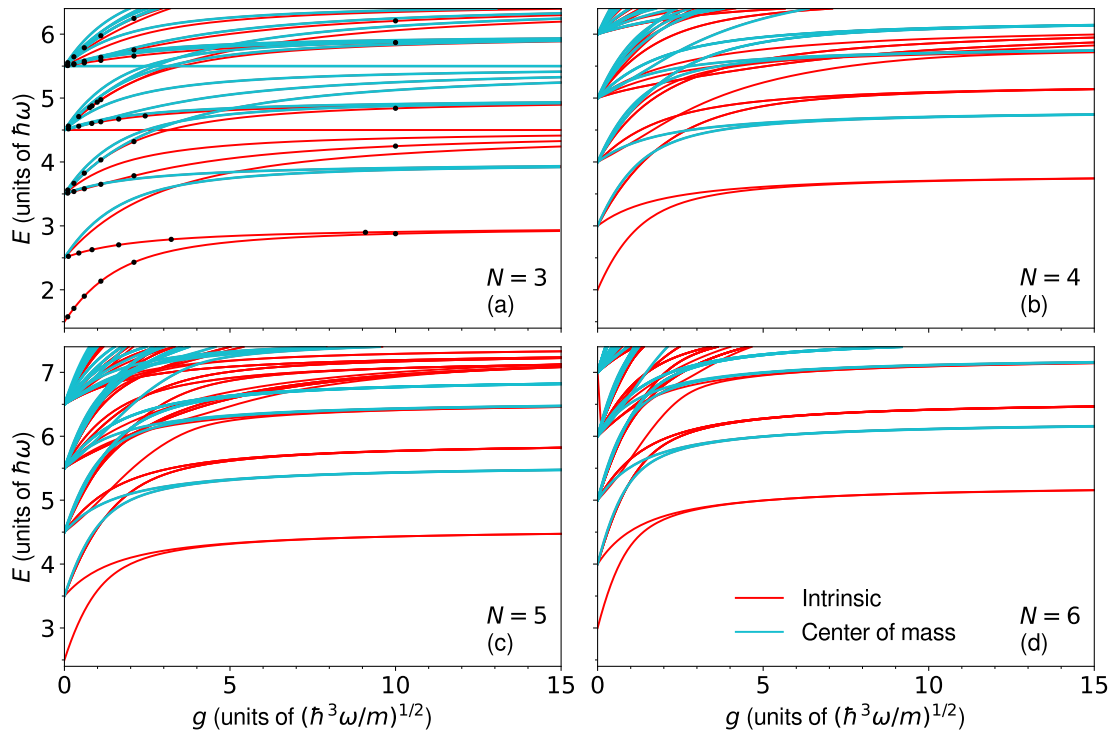


Figure 2. Low-energy spectrum E of three (a), four (b), five (c), and six (d) particles, including the interacting impurity, as a function of the interaction strength g . The solid lines correspond to results from ED while the black circles correspond to the calculation from [35]. We use 90, 45, 30, and 20 HO modes for the three, four, five, and six particles, respectively. The solid red lines correspond to the ground state and the intrinsic excitations, while the blue lines correspond to the center-of-mass excitations.

Note that the first intrinsic excited doublet (for $N > 3$) and the ground state have a similar structure. Therefore, to further examine these states, in figure 3 we show the impurity energy E_I for the ground state doublet and the first intrinsic excited doublet computed by both ED (left panels) and the mean-field solution (right panels) described in section 2.1. For the excitations, E_I is defined as the difference between the energy of the excited state and the energy of the non-interacting ground state.

As discussed in section 3.1, the ground-state energy (see panel (a) of figure 3) in the infinite interacting limit increases with N . Also, the gap between the two states closes for a weaker interaction as the number of particles increases. Independently of N , each state of these doublets has no degeneracy and there is one even and the other with odd parity.

The first intrinsic excited doublet (see panel (c) of figure 3) has the same effects as the ground state: as the number of particles increases the value of the energy in the infinite interacting limit increases and the gap between the two states close for a weaker interaction. Each line of the excited doublet is $N - 2$ times degenerate, and all of the states of one line have either even parity or odd parity.

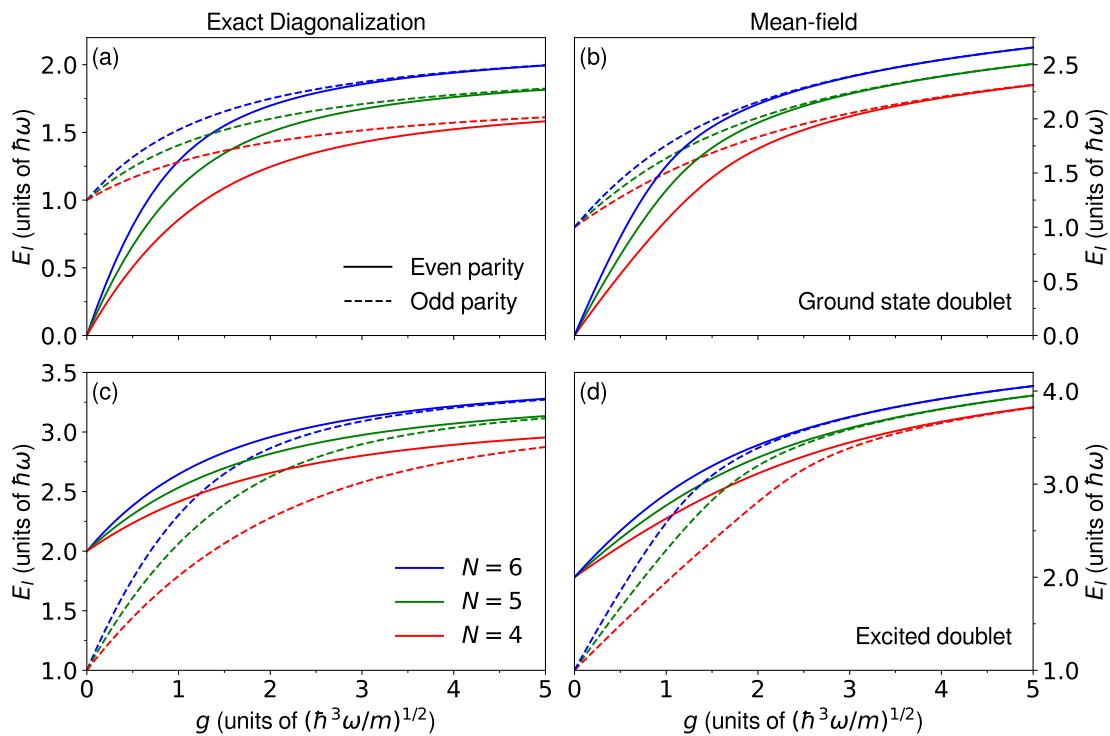


Figure 3. Low-energy E_I spectrum structure for the two lowest doublets for $N = 4, 5,$ and 6 . Panels (a) and (c) correspond to results obtained with exact diagonalization, whereas panels (b) and (d) correspond to mean-field solutions. Panels (a) and (b) show the ground-state doublet, while panels (c) and (d) show the first excited doublet. Solid lines correspond to states with even parity and the dashed lines to states with odd parity.

Nevertheless, if we compare both doublets (panels (a) and (c) of figure 3) we note that the excited ones close their gap for a larger value of the interaction compared with the ground-state doublet. The energy difference between the two doublets in the infinite interacting limit is larger than $\hbar\omega$. This indicates that the excited doublet gains more energy from zero to infinite interaction than the ground state.

We can interpret both doublet states with a simple model in which the impurity is immersed in a double well, where the central barrier is created by the repulsive bath. The height of the central barrier naturally depends on the number of bath particles and on the interaction strength. The Hamiltonian of this one-particle effective model is,

$$H = -\frac{\hbar^2}{2m} \frac{d^2}{dx^2} + \frac{m\omega^2}{2} x^2 + gN_b |\varphi(x)|^2, \quad (15)$$

where we can take $\varphi(x)$ as the harmonic oscillator ground state wavefunction. Note that our mean-field approach is a direct variation of this model, where we introduce the possibility to adapt the central barrier created by the bath particles. In this model, the two lowest states become degenerate when the barrier becomes infinite and they have opposite parity. For this reason, we can understand the doublet states as the ground state and the first excitation of the impurity in the double well. This interpretation

is also useful to explain the excited doublet. In that case, we can understand it as an excitation of the central barrier. This produces a wider central barrier, whose effects are to increase the energy in the infinite interacting limit and to close the gap for larger values of the interaction.

To test our double-well model, we compute the four states corresponding to both doublets with the mean-field solution [(3) and (4)]. The connection between these two models is simple. The excitations of the particle in the double well means excitations of the impurity in the MF, and the excitation of the central barrier in the double-well model is an excitation of one bath particle in the MF. We present the energy of the ground state and an impurity excited state in panel (b) and the energy of a bath particle excited state and both (a bath particle and the impurity) excited state in panel (d) of figure 3, corresponding to the four states obtained with the ED.

Using the self-consistent mean-field technique we obtain that the ground state, see panel (b) of figure 3, does not converge to finite energy in the limit of infinite interaction. In this same panel, we can also note that the state with an impurity excitation also diverges for large interactions. Nevertheless, both states degenerate for large interaction strength. The ground state has even parity whereas the state with an impurity excitation has odd parity. We find the same doublet structure for a different number of particles. As we increase the number of particles, we can appreciate that the gap between the two states closes for weaker interactions. In addition, for large interactions, the doublet reaches higher energies for more populated baths. Similarly, the mean-field excited doublet shows similar behavior to that of the ground-state doublet. Nevertheless, and despite the similarities, ground- and excited-state doublets show some differences. First of all, this excited doublet reaches more energy gain for a fixed large interaction. Secondly, and maybe most remarkable, the excited doublet's gap closes for a larger interaction strength than that of the ground-state doublet.

Despite the energies obtained with the mean-field (see panels (b) and (d) of figure 3) do not coincide with the values computed with ED (see panels (a) and (c) of figure 3), the doublets have the same structure as we described before. So, this shows that the double well interpretation is at least qualitatively in agreement with our calculations.

4. Ground-state density profiles

In this section, we examine the density profiles of the ground state. This enables us to further understand the behavior of the particles across different interaction strengths, and better explain some of the results that we found previously.

We first show the ground-state density profiles obtained from ED for three, four, five, and six particles in figure 4. We show profiles for the impurity (solid lines) and the bath's particles (dash-dotted lines). Note that in the ground state, the profiles of all the bath particles are equal. We show results for a representative set of interaction strengths, where the four left panels correspond to a weak repulsion, the four right panels to essentially the infinite repulsion limit, and the middle panels correspond to intermediate

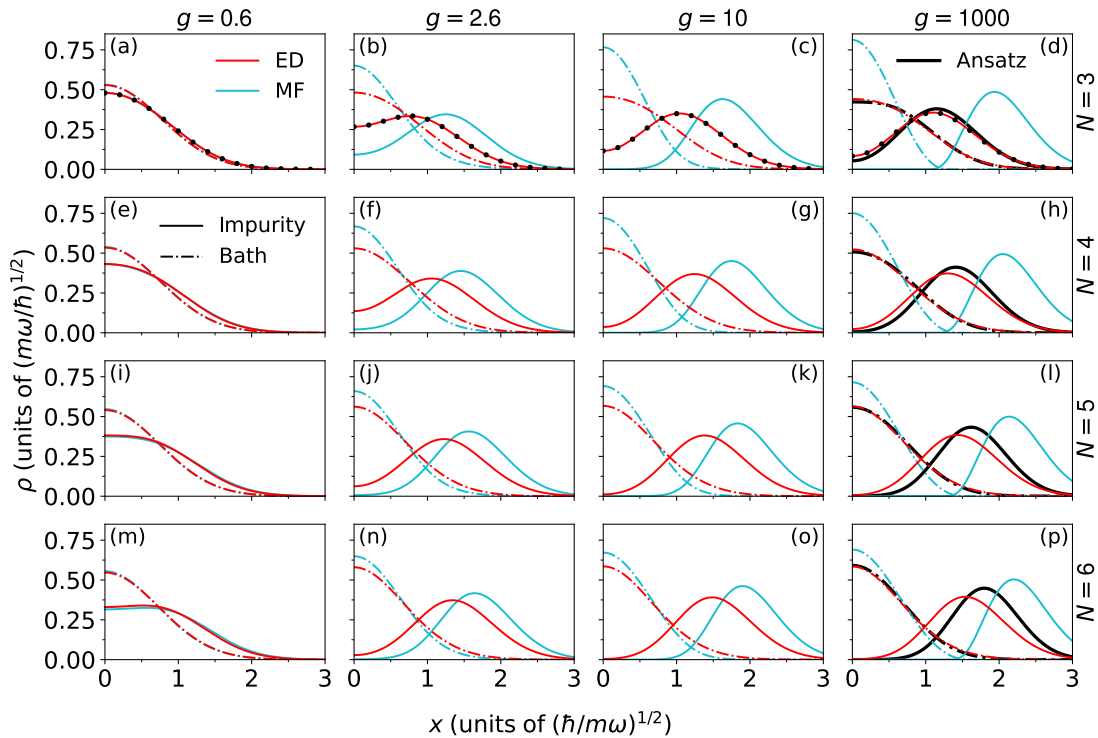


Figure 4. Density of the ground state for three (a, b, c, d), four (e, f, g, h), five (i, j, k, l), and six (m, n, o, p) particles for a selection of interaction strengths g . Each column corresponds to results for a chosen interaction strength g , as indicated at the top of the figure, with g in units of $(\hbar^3\omega/m)^{1/2}$. The solid lines correspond to the density of the impurity, whereas the dash-dotted lines correspond to the density of one of the bath particles. The red lines correspond to ED calculations, the blue lines correspond to MF solutions, and the black lines in the right panels correspond to the densities predicted by ansatz (6) for infinite repulsion. Additionally, the black circles in the top panels correspond to the impurity's density reported in [35] for $N = 3$. Note that for small interactions ($g = 0.6$) the MF results are almost indistinguishable from the ED results.

configurations. To contrast our calculations, we also show the corresponding MF solutions (blue lines) and the ansatz for infinite repulsion (black lines). We also compare with the results from Ref. [35] for $N = 3$, which show a perfect agreement with our ED calculations. Note that the profiles are symmetric with respect to x .

For $g = 0$ (left panels), all the particles are in the HO ground state and thus the profiles are simply Gaussian functions. As the interaction strength increases, the density of the impurity starts developing a two-peak structure, with a minimum at the center of the trap ($x = 0$). In contrast, the bath particles develop a complementary density, with a maximum at the center of the trap. Therefore, the bath remains at the center of the trap, acting as a barrier that pushes the impurity to the edges of the trap. This results in an effective double well-like potential for the impurity, as discussed previously.

As the number of particles increases, we observe that, for a fixed g , the impurity is further repelled from the center of the trap, as can be expected from a system with

a larger repulsive bath. In the same way, the perturbation of the impurity on the bath becomes smaller. From a MF point of view, the strength of the central barrier created by the bath is proportional to the product of the interaction strength and the number of bath particles.

For the three particle cases, we also show the results from Ref. [35] for the impurity density. We compare their results for finite values of the interaction ($g = 0.6, 2.6,$ and 10 , in units of $(m/\hbar^3\omega)^{1/2}$) with our results for the same interactions. We also compare their analytical density for $g = \infty$ with our calculations using $g/(m/\hbar^3\omega)^{1/2} = 1000$. The agreement is almost perfect for all cases.

We also compare the ansatz (6) with the values obtained for the largest interaction (right panels). While there is some noticeable disagreement between the ED calculations and ansatz's solution, they are qualitatively comparable. This shows that our ansatz correctly captures the main features of the wavefunctions. Similarly, the results obtained with the MF approach are almost identical to the ED ones for weak interactions, e.g. $g = 0.6$. In contrast, for larger interactions, the MF densities differ noticeably from those computed with ED, showing larger deviations for strong interactions and smaller baths. In particular, for $N = 3$ and $g = 1000$ (panel d), the MF impurity's density vanishes around $x = 0$, while the ED profile is finite for all values of x . Nevertheless, the MF and ED results are qualitatively in agreement, even in the limit of strong repulsion: the bath particles remain in the center of the trap and the impurity is pushed away, showing a two-peak structure.

In order to further characterize the double well interpretation, in figure 5 we show the position of the maximum of the impurity's density $|x_{\rho_{\max}}|$ as a function of the product between the interaction strength g and the number of bath's particles N_b . We show results obtained numerically with ED (markers) and the corresponding MF solutions (dashed lines) as obtained from (3) and (4). We stress that, as explained before, gN_b dictates the height of the effective central barrier. We also note that we consider the absolute value of $x_{\rho_{\max}}$ because the system is symmetric with respect to x .

While the MF solutions deviate considerably from the ED results, they both show the same qualitative behavior. Indeed, both the ED and MF results predict that, for small g , the impurity's density has only one maximum at the center of the trap, and therefore $x_{\rho_{\max}} = 0$ (left region in the figure). However, the impurity's density develops two symmetric peaks at interaction strengths larger than a critical strength g^* , as illustrated by the appearance of a finite $x_{\rho_{\max}}$ (right region). These two peaks develop suddenly at g^* , and thus $x_{\rho_{\max}}$ shows a discontinuous derivative.

Interestingly, the critical point g^*N_b depends weakly on the number of particles N , and this dependence decreases with increasing N . Indeed, we find that for larger baths the ED critical point converges to $g^*N_b/(\hbar^3\omega/m)^{1/2} \approx 2.5$. Therefore, the impurity shows a seemingly universal transition between being localized at the center of the trap and being expelled to its border. Naturally, this transition should be examined further in the future with robust many-body approaches.

We also find that $|x_{\rho_{\max}}|$ saturates to a finite value in the limit of large repulsion

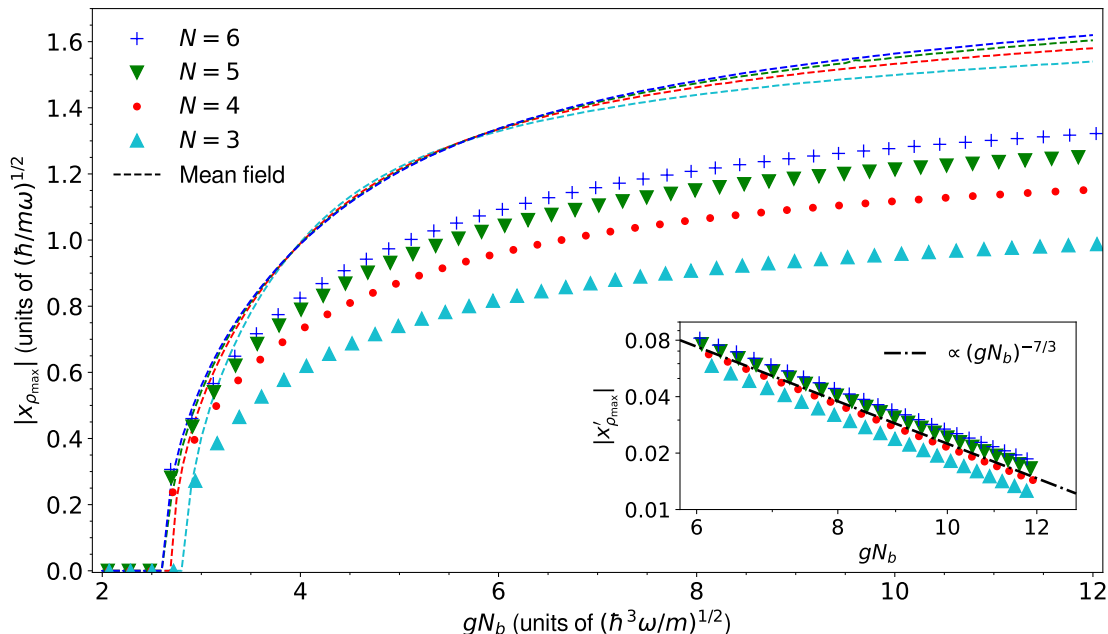


Figure 5. Position of the impurity's density's maximum $x_{\rho_{\max}}$ as a function of gN_b . The markers correspond to numerical results obtained with ED, whereas the dashed lines correspond to MF solutions. The inset shows the derivative of $x_{\rho_{\max}}$ with respect to gN_b in a double logarithmic scale. The dash-dotted line in the inset is an eye guide that shows the power law of the derivatives.

$gN_b \rightarrow \infty$ for both ED and MF results. To show this convergence, we show the derivative of $|x_{\rho_{\max}}|$ obtained from ED in the inset of figure 5 (note the logarithmic scale). It is easy to see that the derivative behaves as a power law. Indeed, we find that it behaves approximately as $\sim 1/(gN_b)^{7/3}$ (see dashed line). Therefore, we can conclude that $|x_{\rho_{\max}}|$ saturate to finite values. Moreover, and as with g^*N_b , the saturation position depends on N , but this dependence decreases with increasing N .

5. Conclusions

In this article, we have examined the energy spectrum and density profiles of the system of an impurity immersed in a bath of a few non-interacting distinguishable particles. We have performed exhaustive numerical diagonalizations to examine a wide range of repulsive impurity-bath interaction strengths and baths with a set of different numbers of particles N . The system shows a rich non-trivial behavior at finite interaction strengths. In particular, we have found that the ground-state impurity energy in the infinite repulsive limit saturates for large N , showing that the energy required to add an impurity to the bath becomes independent of the size of the bath.

We have studied both weak and strong interaction regimes. We have used a mean-field approximation in order to describe the physics when the interactions are small and we have proposed an ansatz for the infinite interacting limit. Both techniques are in

agreement with our exact diagonalization calculations.

Via the energy spectrum, we have identified a double-well behavior in the ground state doublet, that closes the energy gap as the interaction becomes infinite. In addition, we have identified some excited states with similar behavior. These states can be interpreted as a single-particle effective model, where the impurity is immersed in a double well potential, where the central barrier is created by the bath particles. We use a mean-field approach based on this simple model but it allows the central barrier to change due to the interaction. As a consequence, it explains that the impurity for large repulsive interactions is pushed away and becomes localized at the edge of the trap.

By examining the density profiles, we find that the impurity shows a transition between being localized at the center of the trap for weak repulsion, to being expelled to the border of the trap for strong repulsion. The latter corresponds to the double-well regime. Furthermore, we find that the transition manifests at a seemingly universal critical point $g^* N_b$.

Having studied the problem of a single impurity immersed in a non-interacting bath, we devise several future-related extensions of this work. One natural extension is to consider interacting baths, particularly those composed of two-component fermions, as recently studied in homogeneous configurations [42,52]. Consideration of two impurities is also of interest [53], especially due to its connection to the bipolaron problem [54]. Finally, the findings of this work could be further examined in the future for larger baths using robust many-body approaches, such as with quantum Monte-Carlo.

Acknowledgements

We thank J. Martorell for the useful discussions and for carefully reading our manuscript. We thank G. Astrakharchik for useful comments and discussions. We also thank A. Volosniev for providing us the data from [35].

Funding information This work has been funded by Grant No. PID2020-114626GB-I00 from the MICIN/AEI/10.13039/501100011033. F.I. acknowledges funding from EPSRC (UK) through Grant No. EP/V048449/1.

Appendix A. Analytical ansatz calculations

In this appendix, we show some explicit calculations and results of the ansatz (6). First, we develop the calculation of the energy and at the end we show the explicit ansatz functions for four and five particles.

To obtain the value of σ in (6) that minimizes the energy, we need to determine how the energy depends on this parameter. First of all, we compute the normalization constant α_N . Note that all the terms in the sum will give the same σ contribution. For this reason, to simplify the notation, we will show only the case without absolute values.

$$1 = \langle \Psi_{N,\sigma} | \Psi_{N,\sigma} \rangle$$

$$\begin{aligned}
 &= \alpha_N(\sigma) \int e^{-x_I^2/\sigma^2} \prod_{i=1}^{N_b} [(x_I - x_i)^2 e^{-x_i^2/\sigma^2} dx_i] dx_I \\
 &= \alpha_N(\sigma) \int e^{-y_I^2} \prod_{i=1}^{N_b} [(\sigma y_I - \sigma y_i)^2 e^{-y_i^2} \sigma dy_i] \sigma dy_I \\
 &= \sigma^{3N_b+1} \alpha_N(\sigma) \int e^{-y_I^2} \prod_{i=1}^{N_b} [(y_I - y_i)^2 e^{-y_i^2} dy_i] dy_I \\
 &= \sigma^{3N_b+1} \alpha_N(\sigma) \langle \Psi_{N,1} | \Psi_{N,1} \rangle.
 \end{aligned} \tag{A.1}$$

From this result, we obtain the normalization dependence on σ ,

$$\alpha_N(\sigma) = \sigma^{-3N+2} / \langle \Psi_{N,1} | \Psi_{N,1} \rangle. \tag{A.2}$$

Once we have this result, it is the moment to compute the energy. We use compute each contribution of the energy, the kinetic and the potential terms, separately. We define kinetic energy as $\langle \Psi_{N,\sigma} | \sum_i -\frac{1}{2} \frac{\partial^2}{\partial x_i^2} | \Psi_{N,\sigma} \rangle$ and the potential energy as $\langle \Psi_{N,\sigma} | \sum_i \frac{1}{2} x_i^2 | \Psi_{N,\sigma} \rangle$. The dependence of these energies with σ is also possible to obtain analytically with the same procedure as the normalization, being the kinetic one

$$\begin{aligned}
 E_{\text{kin.}}(\sigma) &= \alpha_N(\sigma) \int e^{-x_I^2/\sigma^2} \prod_{j=1}^{N_b} [(x_I - x_j) e^{-x_j^2/2\sigma^2}] \sum_k \left(\frac{-1}{2} \frac{\partial^2}{\partial x_k^2} \right) \\
 &\quad \times \prod_{i=1}^{N_b} [(x_I - x_i) e^{-x_i^2/2\sigma^2} dx_i] dx_I \\
 &= \sigma^{-2} E_{\text{kin.}}(1),
 \end{aligned} \tag{A.3}$$

and for the potential energy,

$$\begin{aligned}
 E_{\text{pot.}}(\sigma) &= \alpha_N(\sigma) \int e^{-x_I^2/\sigma^2} \prod_{j=1}^{N_b} [(x_I - x_j) e^{-x_j^2/2\sigma^2}] \sum_k \frac{1}{2} x_k^2 \\
 &\quad \times \prod_{i=1}^{N_b} [(x_I - x_i) e^{-x_i^2/2\sigma^2} dx_i] dx_I \\
 &= \sigma^2 E_{\text{pot.}}(1).
 \end{aligned} \tag{A.4}$$

With these results, the total energy can be expressed as a function of the σ parameter as

$$E(\sigma) = \sigma^2 E_{\text{pot.}}(1) + \sigma^{-2} E_{\text{kin.}}. \tag{A.5}$$

As a consequence of the variational theorem, we know that the energy will be an upper bound of the exact value. For this reason, we are interested in the minimal value of the energy obtained by changing the variational parameter. By minimizing the energy, we obtain the optimal value of σ , and then the energy for that optimal value.

$$\left. \frac{\partial E}{\partial \sigma} \right|_{\sigma_{\text{opt.}}} = 0 \tag{A.6}$$

$$2\sigma_{\text{opt.}} E_{\text{pot.}}(1) - 2\sigma_{\text{opt.}}^{-3} E_{\text{kin.}}(1) = 0 \tag{A.7}$$

$$\sigma_{\text{opt.}} = \left(\frac{E_{\text{kin.}}(1)}{E_{\text{pot.}}(1)} \right)^{1/4}. \tag{A.8}$$

Here we define $E_{\text{pot.}}(1) \equiv E_{\text{pot.}}$ and $E_{\text{kin.}}(1) \equiv E_{\text{kin.}}$, and finally, the minimum energy obtained with the optimal variational parameter is

$$E(\sigma_{\text{opt.}}) = \sigma_{\text{opt.}}^2 E_{\text{pot.}} + \sigma_{\text{opt.}}^{-2} E_{\text{kin.}} \quad (\text{A.9})$$

$$E(\sigma_{\text{opt.}}) = \sqrt{\frac{E_{\text{kin.}}}{E_{\text{pot.}}}} E_{\text{pot.}} + \sqrt{\frac{E_{\text{pot.}}}{E_{\text{kin.}}}} E_{\text{kin.}} \quad (\text{A.10})$$

$$E(\sigma_{\text{opt.}}) = 2\sqrt{E_{\text{kin.}} E_{\text{pot.}}} . \quad (\text{A.11})$$

To clarify the ansatz that we use, here we present the explicit expression for four and five particles. The expression for three particles is on the main text in (9). For four particles, the ansatz reads,

$$\begin{aligned} |\Psi_4, \sigma\rangle = \exp \left[\left(-x_I^2 - x_A^2 - x_B^2 - x_C^2 \right) / 2\sigma^2 \right] & [(x_I - x_A)|x_I - x_B||x_I - x_C| \\ & + (x_I - x_B)|x_I - x_A||x_I - x_C| + (x_I - x_C)|x_I - x_A||x_I - x_B| \\ & + (x_I - x_A)(x_I - x_B)(x_I - x_C)] , \end{aligned} \quad (\text{A.12})$$

and for five particles, the ansatz reads,

$$\begin{aligned} |\Psi_5, \sigma\rangle = \exp \left[\left(-x_I^2 - x_A^2 - x_B^2 - x_C^2 - x_D^2 \right) / 2\sigma^2 \right] & \\ \times [|x_I - x_A||x_I - x_B||x_I - x_C||x_I - x_D| & \\ + (x_I - x_A)(x_I - x_B)|x_I - x_C||x_I - x_D| & \\ + (x_I - x_A)(x_I - x_C)|x_I - x_B||x_I - x_D| & \\ + (x_I - x_B)(x_I - x_C)|x_I - x_A||x_I - x_D| & \\ + (x_I - x_A)(x_I - x_D)|x_I - x_B||x_I - x_C| & \\ + (x_I - x_B)(x_I - x_D)|x_I - x_A||x_I - x_C| & \\ + (x_I - x_C)(x_I - x_D)|x_I - x_A||x_I - x_B| & \\ + (x_I - x_A)(x_I - x_B)(x_I - x_C)(x_I - x_D)] . & \end{aligned} \quad (\text{A.13})$$

- [1] Landau L and Pekar S 1948 *Zh. Eksp. Teor. Fiz* **18** 419–423
- [2] Girardeau M 1961 *Physics of Fluids* **4** 279 ISSN 00319171 URL <https://aip.scitation.org/doi/10.1063/1.1706323>
- [3] Fabrocini A and Polls A 1998 *Physical Review B* **58** 5209–5212 publisher: American Physical Society URL <https://link.aps.org/doi/10.1103/PhysRevB.58.5209>
- [4] Kutschera M and Wójcik W 1993 *Physical Review C* **47** 1077–1085 publisher: American Physical Society URL <https://link.aps.org/doi/10.1103/PhysRevC.47.1077>
- [5] Bloch I, Dalibard J and Zwerger W 2008 *Reviews of Modern Physics* **80** 885–964 publisher: American Physical Society URL <https://link.aps.org/doi/10.1103/RevModPhys.80.885>
- [6] Bloch I, Dalibard J and Nascimbène S 2012 *Nature Physics* **8** 267–276 ISSN 1745-2481 number: 4 Publisher: Nature Publishing Group URL <https://www.nature.com/articles/nphys2259>
- [7] Schirotzek A, Wu C H, Sommer A and Zwierlein M W 2009 *Physical Review Letters* **102** 230402 publisher: American Physical Society URL <https://link.aps.org/doi/10.1103/PhysRevLett.102.230402>
- [8] Nascimbène S, Navon N, Jiang K J, Tarruell L, Teichmann M, McKeever J, Chevy F and Salomon C 2009 *Physical Review Letters* **103** 170402 publisher: American Physical Society URL <https://link.aps.org/doi/10.1103/PhysRevLett.103.170402>
- [9] Jørgensen N B, Wacker L, Skalmstang K T, Parish M M, Levinsen J, Christensen R S, Bruun G M and Arlt J J 2016 *Physical Review Letters* **117** 055302 publisher: American Physical Society URL <https://link.aps.org/doi/10.1103/PhysRevLett.117.055302>
- [10] Hu M G, Van de Graaff M J, Kedar D, Corson J P, Cornell E A and Jin D S 2016 *Physical Review Letters* **117** 055301 publisher: American Physical Society URL <https://link.aps.org/doi/10.1103/PhysRevLett.117.055301>
- [11] Vlietinck J, Ryckebusch J and Van Houcke K 2013 *Physical Review B* **87** 115133 publisher: American Physical Society URL <https://link.aps.org/doi/10.1103/PhysRevB.87.115133>
- [12] Christensen R S, Levinsen J and Bruun G M 2015 *Physical Review Letters* **115** 160401 publisher: American Physical Society URL <https://link.aps.org/doi/10.1103/PhysRevLett.115.160401>
- [13] Volosniev A G and Hammer H W 2017 *Physical Review A* **96** 031601 publisher: American Physical Society URL <https://link.aps.org/doi/10.1103/PhysRevA.96.031601>
- [14] Koschorreck M, Pertot D, Vogt E, Fröhlich B, Feld M and Köhl M 2012 *Nature* **485** 619–622 ISSN 1476-4687 number: 7400 Publisher: Nature Publishing Group URL <https://www.nature.com/articles/nature11151>
- [15] Ardila L A P, Astrakharchik G E and Giorgini S 2020 *Physical Review Research* **2** 023405 publisher: American Physical Society URL <https://link.aps.org/doi/10.1103/PhysRevResearch.2.023405>
- [16] Hryhorchak O, Panochko G and Pastukhov V 2020 *Journal of Physics B: Atomic, Molecular and Optical Physics* **53** 205302 ISSN 0953-4075 publisher: IOP Publishing URL <https://dx.doi.org/10.1088/1361-6455/abb3ab>
- [17] Giamarchi T 2004 *Quantum Physics in One Dimension* International Series of Monographs on Physics (Oxford University Press) ISBN 978-0-19-852500-4
- [18] Mistakidis S I, Volosniev A G, Barfknecht R E, Fogarty T, Busch T, Foerster A, Schmelcher P and Zinner N T 2022 Cold atoms in low dimensions – a laboratory for quantum dynamics arXiv:2202.11071 [cond-mat, physics:physics, physics:quant-ph] URL <http://arxiv.org/abs/2202.11071>
- [19] Chen J, Mistakidis S I and Schmelcher P 2022 *New Journal of Physics* **24** 033004 ISSN 1367-2630 publisher: IOP Publishing URL <https://dx.doi.org/10.1088/1367-2630/ac51ed>
- [20] Grusdt F, Astrakharchik G E and Demler E 2017 *New Journal of Physics* **19** 103035 ISSN 1367-2630 publisher: IOP Publishing URL <https://dx.doi.org/10.1088/1367-2630/aa8a2e>
- [21] Will M, Astrakharchik G and Fleischhauer M 2021 *Physical Review Letters* **127** 103401 publisher: American Physical Society URL <https://link.aps.org/doi/10.1103/PhysRevLett.127.103401>

103401

- [22] Petković A and Ristivojevic Z 2016 *Physical Review Letters* **117** 105301 publisher: American Physical Society URL <https://link.aps.org/doi/10.1103/PhysRevLett.117.105301>
- [23] Brauneis F, Hammer H W, Lemeshko M and Volosniev A 2021 *SciPost Physics* **11** 008 ISSN 2542-4653 URL <https://scipost.org/SciPostPhys.11.1.008>
- [24] Keiler K, Mistakidis S I and Schmelcher P 2020 *New Journal of Physics* **22** 083003 ISSN 1367-2630 publisher: IOP Publishing URL <https://dx.doi.org/10.1088/1367-2630/ab9e34>
- [25] Massel F, Kantian A, Daley A J, Giamarchi T and Törmä P 2013 *New Journal of Physics* **15** 045018 ISSN 1367-2630 publisher: IOP Publishing URL <https://dx.doi.org/10.1088/1367-2630/15/4/045018>
- [26] Burovski E, Gamayun O and Lychkovskiy O 2021 Mobile impurity in a one-dimensional quantum gas: Exact diagonalization in the Bethe Ansatz basis arXiv:2112.06627 [cond-mat] URL <http://arxiv.org/abs/2112.06627>
- [27] Yordanov V R and Isaule F 2023 *Journal of Physics B: Atomic, Molecular and Optical Physics* **56** 045301 ISSN 0953-4075 publisher: IOP Publishing URL <https://dx.doi.org/10.1088/1361-6455/acb51b>
- [28] Bethe H 1931 *Zeitschrift für Physik* **71** 205–226 ISSN 0044-3328 URL <https://doi.org/10.1007/BF01341708>
- [29] Raventós D, Graß T, Lewenstein M and Juliá-Díaz B 2017 *Journal of Physics B: Atomic, Molecular and Optical Physics* **50** 113001 ISSN 0953-4075 publisher: IOP Publishing URL <https://dx.doi.org/10.1088/1361-6455/aa68b1>
- [30] Weiße A and Fehske H 2008 Exact Diagonalization Techniques *Computational Many-Particle Physics* Lecture Notes in Physics ed Fehske H, Schneider R and Weiße A (Berlin, Heidelberg: Springer) pp 529–544 ISBN 978-3-540-74686-7 URL https://doi.org/10.1007/978-3-540-74686-7_18
- [31] Paredes B, Widera A, Murg V, Mandel O, Fölling S, Cirac I, Shlyapnikov G V, Hänsch T W and Bloch I 2004 *Nature* **429** 277–281 ISSN 1476-4687 number: 6989 Publisher: Nature Publishing Group URL <https://www.nature.com/articles/nature02530>
- [32] Kinoshita T, Wenger T and Weiss D S 2004 *Science (New York, N.Y.)* **305** 1125–1128 ISSN 1095-9203
- [33] Catani J, Lamporessi G, Naik D, Gring M, Inguscio M, Minardi F, Kantian A and Giamarchi T 2012 *Physical Review A* **85** 023623 publisher: American Physical Society URL <https://link.aps.org/doi/10.1103/PhysRevA.85.023623>
- [34] Dehkharghani A S, Volosniev A G and Zinner N T 2015 *Physical Review A* **92** 031601 publisher: American Physical Society URL <https://link.aps.org/doi/10.1103/PhysRevA.92.031601>
- [35] Zinner N T, Volosniev A G, Fedorov D V, Jensen A S and Valiente M 2014 *Europhysics Letters* **107** 60003 ISSN 0295-5075 publisher: EDP Sciences, IOP Publishing and Società Italiana di Fisica URL <https://dx.doi.org/10.1209/0295-5075/107/60003>
- [36] Mistakidis S, Katsimiga G, Koutentakis G, Busch T and Schmelcher P 2019 *Physical Review Letters* **122** 183001 publisher: American Physical Society URL <https://link.aps.org/doi/10.1103/PhysRevLett.122.183001>
- [37] Mistakidis S I, Katsimiga G C, Koutentakis G M and Schmelcher P 2019 *New Journal of Physics* **21** 043032 ISSN 1367-2630 publisher: IOP Publishing URL <https://dx.doi.org/10.1088/1367-2630/ab1045>
- [38] Dehkharghani A, Volosniev A and Zinner N 2018 *Physical Review Letters* **121** 080405 publisher: American Physical Society URL <https://link.aps.org/doi/10.1103/PhysRevLett.121.080405>
- [39] Mistakidis S I, Volosniev A G, Zinner N T and Schmelcher P 2019 *Physical Review A* **100** 013619 publisher: American Physical Society URL <https://link.aps.org/doi/10.1103/PhysRevA.100.013619>
- [40] Włodzyński D 2022 *Physical Review A* **106** 033306 publisher: American Physical Society URL

- <https://link.aps.org/doi/10.1103/PhysRevA.106.033306>
- [41] Mistakidis S I, Koutentakis G M, Katsimiga G C, Busch T and Schmelcher P 2020 *New Journal of Physics* **22** 043007 ISSN 1367-2630 publisher: IOP Publishing URL <https://dx.doi.org/10.1088/1367-2630/ab7599>
- [42] Rammelmüller L, Huber D, Čufar M, Brand J, Hammer H W and Volosniev A G 2023 *SciPost Physics* **14** 006 ISSN 2542-4653 URL <https://scipost.org/10.21468/SciPostPhys.14.1.006>
- [43] García-March M A, Dehkharghani A S and Zinner N T 2016 *Journal of Physics B: Atomic, Molecular and Optical Physics* **49** 075303 ISSN 0953-4075 publisher: IOP Publishing URL <https://doi.org/10.1088/0953-4075/49/7/075303>
- [44] Deuretzbacher F, Bongs K, Sengstock K and Pfannkuche D 2007 *Physical Review A* **75** 013614 publisher: American Physical Society URL <https://link.aps.org/doi/10.1103/PhysRevA.75.013614>
- [45] Kościk P 2018 *Physics Letters A* **382** 2561–2564 ISSN 0375-9601 URL <https://www.sciencedirect.com/science/article/pii/S0375960118306947>
- [46] Rojo-Francàs A, Polls A and Juliá-Díaz B 2020 *Mathematics* **8** 1196 number: 7 Publisher: Multidisciplinary Digital Publishing Institute URL <https://www.mdpi.com/2227-7390/8/7/1196>
- [47] Rojo-Francàs A, Isaule F and Juliá-Díaz B 2022 *Physical Review A* **105** 063326 publisher: American Physical Society URL <https://link.aps.org/doi/10.1103/PhysRevA.105.063326>
- [48] Płodzień M, Wiater D, Chrostowski A and Sowiński T 2018 Numerically exact approach to few-body problems far from a perturbative regime arXiv:1803.08387 [cond-mat] URL <http://arxiv.org/abs/1803.08387>
- [49] Jastrow R 1955 *Physical Review* **98** 1479–1484 publisher: American Physical Society URL <https://link.aps.org/doi/10.1103/PhysRev.98.1479>
- [50] Barth M and Zwerger W 2011 *Annals of Physics* **326** 2544–2565 ISSN 0003-4916 URL <https://www.sciencedirect.com/science/article/pii/S0003491611001084>
- [51] Busch T, Englert B G, Rzazewski K and Wilkens M 1998 *Foundations of Physics* **28** 549–559 ISSN 1572-9516 URL <https://doi.org/10.1023/A:1018705520999>
- [52] Pierce M, Leyronas X and Chevy F 2019 *Physical Review Letters* **123** 080403 publisher: American Physical Society URL <https://link.aps.org/doi/10.1103/PhysRevLett.123.080403>
- [53] Theel F, Mistakidis S I and Schmelcher P 2023 Crossover from attractive to repulsive induced interactions and bound states of two distinguishable Bose polarons arXiv:2303.04699 [cond-mat] URL <http://arxiv.org/abs/2303.04699>
- [54] Camacho-Guardian A, Peña Ardila L, Pohl T and Bruun G 2018 *Physical Review Letters* **121** 013401 publisher: American Physical Society URL <https://link.aps.org/doi/10.1103/PhysRevLett.121.013401>